A&A 371, 771–778 (2001)
DOI: 10.1051/0004-6361:20010448

Astronomy & Astrophysics

New constraints on the cosmic mid-infrared background using TeV gamma-ray astronomy

C. Renault[1,⋆], A. Barrau[2], G. Lagache[3], and J.-L. Puget[3]

[1] LPNHE, CNRS-IN2P3, Universités Paris VI-VII, 4 place Jussieu, 75252 Paris Cedex 05, France
[2] ISN Grenoble, CNRS-IN2P3, Université Joseph Fourier, 53 Av. des Martyrs, 38026 Grenoble Cedex, France
[3] IAS, Université de Paris XI, 91405 Orsay Cedex, France

Received 13 December 2000 / Accepted 16 February 2001

Abstract. Very high energy gamma-ray data obtained by CAT and HEGRA from the active galactic nucleus Mkn 501 are used to constrain the cosmic Mid-Infrared background. While the entire infrared and submillimeter spectrum shape based on models has been fixed and the density scaled as a whole in previous studies, recent measures on the low and high energy infrared background are extensively used in this paper. In this original approach the infrared distribution is only varied in the unexplored 3.5–100 μm region. With a conservative hypothesis on the intrinsic spectrum of Mkn 501, an upper limit of 4.7 nW m^{-2} sr^{-1} between 5 and 15 μm is derived, which is very close to the lower limit inferred from deep ISOCAM cosmological surveys at 15 μm. This result is shown to be independent of the exact density of the $\lambda < 3.5$ μm and $\lambda > 100$ μm infrared distribution within the uncertainties of the measurements. Moreover, the study presented here rules out a complete extragalactic origin for the 60 micron tentative background detection as found by Finkbeiner et al. (2000).

Key words. diffuse radiation – infrared: general – gamma-rays: observations – BL Lacertae objects: Mkn 501

1. Introduction

Our knowledge of the early epochs of galaxies has recently increased thanks to the observational evidences provided by UV/Vis/Near-IR, far-IR and submillimeter (submm) surveys of high-redshift objects. In a consistent picture, galaxy formation and evolution can also be constrained by the background radiation which is produced by the line-of-sight accumulation of all extragalactic sources.

In the last two years the Extragalactic Background (EB) at visible, IR and submm wavelengths has been finally constrained by both very deep source counts and upper limits on the diffuse isotropic emission at shorter wavelengths, and measurements in the submm range (see Gispert et al. 2000 for a review).

The Cosmic Infrared Background (CIB) detected in the COBE data at wavelengths greater than 100 μm (Fixsen et al. 1998; Hauser et al. 1998; Schlegel et al. 1998; Lagache et al. 1999) contains a surprisingly large fraction of background due to distant galaxies. The spectrum implies that the submm part of the CIB cannot be dominated by the emission of the galaxies, which accounts for most of the CIB at 150 μm, and thus contains unique information about high redshift IR galaxies. Considering the variety of long wavelength spectra observed for these galaxies, Gispert et al. (2000) have shown that a co-moving production rate of far-IR radiation with strong evolution at low redshifts but little evolution between redshifts 1 and 4 is the only solution allowed by the CIB.

The search for the UV, optical, near-IR and mid-IR EB (from 0.2 to 2.2 μm) obtained by summing the contributions of galaxies using number counts currently gives only lower limits; but the flattening of the faint counts suggests that we are now close to convergence. Nevertheless, number counts give a good determination of the background only if the full flux of the sources is properly taken into account (Bernstein et al. 1999) and if diffuse components are negligible. In fact, studies of the diffuse COBE emission (Gorjian et al. 2000; Dwek & Arendt 1998; Cambrésy et al. 2000) suggest that a significant fraction of the EB is missed from number counts integrals in the near-IR.

Due to the bright zodiacal foreground emission (see for example Kellsall et al. 1998), EB determinations from 5 to about 80 μm are very difficult. In this wavelength range, EB constraints come mostly from deep IR cosmological surveys, such as the ones performed with ISOCAM (e.g. Elbaz et al. 1998). A more controversial tentative CIB detection at 60 μm has also been published using DIRBE data (Finkbeiner et al. 2000).

It has been suggested that observations of the TeV spectrum of extragalactic sources can be a powerful tool to constrain the CIB spectrum (Nikishov 1962; Gould & Schreder 1967; Stecker et al. 1992), especially around

Send offprint requests to: C. Renault,
e-mail: rcecile@in2p3.fr
⋆ Now at ISN Grenoble.

10 μm, where the EB constraints are today very weak. TeV gamma rays propagating in the intergalactic medium undergo absorption through electron pair production on CIB photons. Using sources Mkn 421 and Mkn 501, meaningful upper limits have been established (see Malkan & Stecker 1998; Funk et al. 1998; Macminn & Primack 1996; Stanev & Franceschini 1998; Guy et al. 2000 for example).

In this paper, gamma-ray data are used, together with the best presently available direct CIB measurements (rather than CIB models), to improve the constraints in the most difficult spectral region, near the maximum of the zodiacal emission. The paper is organised as follows. We discuss in Sect. 2 the CIB measurements that will be used. Section 3 presents the TeV gamma-ray data. The determination of the upper limit is explained and performed in Sects. 4 and 5. In Sect. 6, we compare our upper limit with lower limits derived from deep source counts obtained with the ISOCAM instrument aboard ISO (Elbaz et al. 1998; Metcalfe et al. 2000) and discuss the CIB distribution shape from 10 to 100 μm. Cosmological implications are then discussed. Finally, in Sect. 7, the consequences for the physical parameters of Mkn 501 of the internal absorption are briefly considered.

2. CIB density distribution

This study aims at deriving upper limits on the minimum of the CIB distribution lying in the Mid-IR (5–80 μm) region. In the Far-IR region, the distribution is constrained to account for the 100 μm determination from Lagache et al. (1999), which is in very good agreement with the value of Finkbeiner et al. (2000); data at longer wavelengths are not relevant for this study as they are beyond the threshold of the hardest TeV photons. In the Near-IR region, three different hypotheses, parametrised in this work by polynomial fits between 0.2 and 3.5 μm, are considered: the first one (dashed-dotted line in Fig. 1, referred as *HDF*) is directly based on Hubble Deep Field galaxy counts (Pozzetti et al. 1998), and can therefore be considered as a lower limit; the second one (full line in Fig. 1, referred as *HDF+spectro*) is derived from *HDF* results combined with ground-based spectrometry (Bernstein et al. 1999) and the third one (dotted line in Fig. 1, referred as *Cambresy*) is based on (Cambrésy et al. 2000) points at 1.25 and 2.2 μm linked to the UV point at 0.2 μm (Bowyer et al. 1991, combined with Armand et al. 1994), as it is clearly incompatible with *HDF* and *HDF + spectro* hypothesis[1]. All these parametrisations are required to agree with the 3.5 μm measurement from Gorjian et al. (2000); the *HDF* and *HDF + spectro* hypothesis also include the 1.25 and 2.2 μm points from Wright (2000).

The CIB coming from the line of sight accumulation of all extragalactic sources is expected to have a smooth spectrum. The CIB might present a minimum between the stellar dominated part and the interstellar dust dominated one between 3 and 15 μm. To make optimum use of the upper limits that TeV gamma rays can provide, we thus use an empirical model for the CIB with a small number of free parameters ($\lambda_{\rm min}$–$f_{\rm min}$) which interpolates between 3.5 and 100 μm two segments of parabola (in log-log plot) linking the 3.5 or 100 μm points to the minimum located at ($\lambda_{\rm min}$, $f_{\rm min}$) with a null first derivative at this point. The CIB empirical density distribution is shown in Fig. 1 for $\lambda_{\rm min} = 10$ μm and $f_{\rm min} = 2$, 4 or 6 nW m^{-2} sr^{-1}.

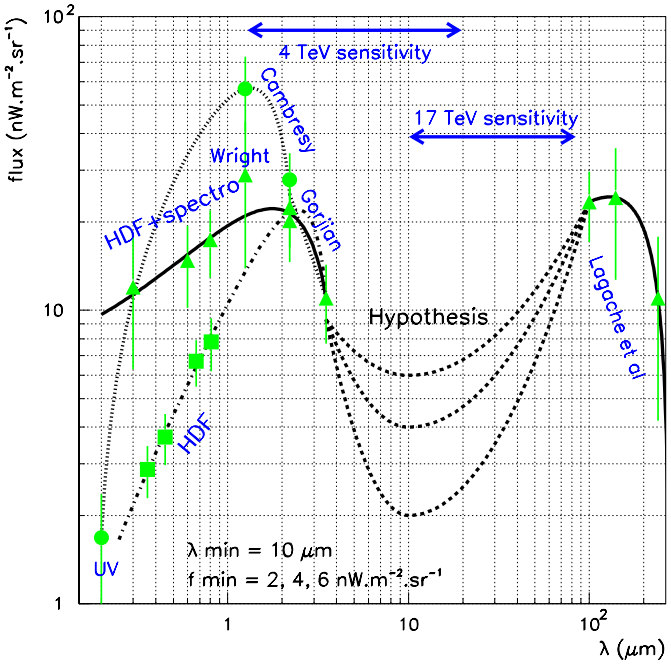

Fig. 1. Assumed shapes of the CIB density distribution between 0.2 and 100 μm. Each profile between 3.5 and 100 μm is characterised by the position of the minimum ($\lambda_{\rm min}, f_{\rm min}$). In this example $\lambda_{\rm min} = 10$ μm. See the text for details. Arrows show the 90% interacting interval of target radiations for a 4 or 17 TeV photon (for $f_{\rm min} = 4$ nW m^{-2} sr^{-1}). The full line links the (*HDF*+spectro) points (0.3 to 0.8 μm), the (Wright 2000) points (1.25 to 2.2 μm) and the (Gorjian et al. 2000) points (2.2 to 3.5 μm). The dashed-dotted line links smoothly the *HDF* points to the (Wright 2000) and (Gorjian et al. 2000) points. The dotted line links the UV measurement at 0.2 μm, the (Cambrésy et al. 2000) points (1.25 to 2.2 μm) and the 3.5 μm (Gorjian et al. 2000) points

3. TeV gamma-ray astronomy data

The TeV source Mkn 501 is the second closest X-ray selected BL Lac object after Mkn 421 with a redshift $z \simeq 0.034$. During the 1997 outburst which lasted several months, Mkn 501 was observed intensively in X-rays (BeppoSAX: Pian et al. 1998, RXTE: Lamer & Wagner 1998) and TeV γ-rays (Whipple: Catanese et al. 1997; Samuelson et al. 1998; HEGRA: Aharonian et al. 1997, 1999a, 1999b; Telescope Array: Hayashida et al. 1998; CAT: Djannati-Ataï et al. 1999). The exceptional April 16, 1997 flare was observed by BeppoSAX and

[1] However, we will see (Sect. 5.2) that the impact of the density below 1 μm is ≈null.

low-energy threshold (∼300 GeV) Whipple and CAT atmospheric Cherenkov telescopes, allowing the derivation of the energy spectrum with good accuracy in a broad dynamical range.

These unique data initiated interesting efforts to set meaningful upper limits on the CIB flux (see Biller et al. 1998; Stanev & Franceschini 1998; Barrau 1998; Stecker & De Jager 1998; Stecker 1999; Aharonian et al. 1999b; Coppi & Aharonian 1999; Konopelko et al. 1999; Guy et al. 2000).

In this paper, CAT and HEGRA data from 400 GeV to 17 TeV are used. Due to bad weather, the HEGRA telescope system could not observe this flare. However, the HEGRA observations of Mkn 501 revealed that, despite flux variations in sub-day time-scales, the shape of the energy spectrum above 1 TeV remained essentially stable throughout the entire state of high activity in 1997. The HEGRA "time-averaged" spectrum (Aharonian et al. 1999b) can therefore be used after normalisation to the CAT April 16, 1997 spectrum at $E = 1$ TeV with the re-scaling factor of ≈2.2 (Guy et al. 2000). At these energies the agreement between the CAT and HEGRA spectra is quite impressive. Below 1 TeV, CAT points are used solely since in this energy region both the statistical and systematic errors of the data obtained close to the energy threshold of the HEGRA telescope system are significantly larger than CAT data uncertainties.

4. Unfolding TeV spectra

The influence of low energy photons in the Universe on the propagation of Very High Energy (VHE) gamma-rays was pointed out by Nikishov (1962). An original way of using ground-based TeV observations of distant sources to probe the CIB was given by Stecker et al. (1992). The fundamental idea is to look for absorption in the intrinsic spectrum as a result of electron-positron pair production by photon collisions $\gamma_{\rm TeV} + \gamma_{\rm CIB} \rightarrow {\rm e}^+ + {\rm e}^-$.

In such an interaction between a gamma-ray of energy $(1+z)E$ and an infrared photon of energy $(1+z)\epsilon$, where z is the redshift, E and ϵ the observed energies at $z = 0$, the pair production threshold is $E\epsilon\,(1+z)^2\,(1-\cos\theta) > 2\left(mc^2\right)^2$ where θ is the angle between photons and m the rest mass of the electron. The cross-section can be written as (Heitler 1960): $\sigma = k\left(1-\beta^2\right)\left(2\beta\left(\beta^2-2\right)+\left(3-\beta^4\right)\ln\left(\frac{1+\beta}{1-\beta}\right)\right)$ cm^2 with $\beta = \left(1-2\left(mc^2\right)^2/\left(E\epsilon\,(1-\cos\theta)\right)(1+z)^2\right)^{1/2}$ and $k = 1.25\ 10^{-25}$. If the infrared photons have a density number $n\,(\epsilon)\,{\rm d}\epsilon$ cm^{-3}, the corresponding optical depth for attenuation is

$$\tau(E) = \frac{c}{H_0}\int_0^{z_{\rm s}} {\rm d}z\,(1+z)^{1/2} \int_{-1}^{1} {\rm d}\,(\cos\theta)\,\tfrac{1-\cos\theta}{2}\int_{\epsilon_{\rm t}}^{\infty} {\rm d}\epsilon\; n(\epsilon)\sigma(E,\epsilon,\theta)$$

where $\epsilon_{\rm t} = 2(mc^2)^2/(E(1-\cos\theta)(1+z)^2)$, $z_{\rm s}$ is the redshift of the source, c the light speed, and H_0 the Hubble parameter (assumed here equal to 65 km s^{-1} Mpc^{-1}). For this equation, the density parameter Ω_0 was chosen close to unity. The detected flux is then attenuated by a factor $\mathrm{e}^{-\tau(E)}$. The CIB energy distribution is assumed to be independent of z as the γ-ray source redshift is very low (0.034).

The maximum cross-section is reached for an infrared photon wavelength of $\lambda_{\rm CIB} \approx \lambda_{\rm c}\frac{E}{2mc^2}$ where $\lambda_{\rm c} = h/(mc)$ is the Compton wavelength of the electron. As shown in Fig. 1, γ-photons with energy between a few TeV and 20 TeV "see" CIB photons with wavelengths between 3.5 and 100 μm.

5. Upper limit on the CIB

5.1. Method

To turn the absorption-corrected spectra into an upper limit on the CIB density, the intrinsic spectral energy density of Mkn 501 is assumed to be convex in the multi-TeV region (Guy et al. 2000). This conservative hypothesis is based on the fact that no natural physical process can re-inject energy above the Inverse-Compton bump maximum. Both Klein-Nishina effect and auto-absorption within the source would cause the flux to decrease more and more rapidly as a function of energy. In the framework of more complex hadronic models this convex shape is also expected, either because of proton-initiated-cascade (often modeled as a broken power-law around 3 TeV), or due to the inclusion of μ-synchrotron radiation (Mannheim, private communication). Even in the extreme case where proton synchrotron radiation is at the origin of the TeV bump (Aharonian 2000), the shape of the emission remains convex.

Looking at the absorption corrected spectra shown in Fig. 2, it cannot be excluded that the maximum of the so-called Inverse-Compton peak is not yet reached at 17 TeV when a large amount of CIB radiation ($f_{\rm min} >$ 6 nW m^{-2} sr^{-1}) is assumed. Physical parameters (essentially magnetic field and Doppler factor) required to produce such a spectral energy distribution maximum above 17 TeV are substantially disfavoured but, even in this case, the $\nu F(\nu)$ shape should remain convex. This latter point is ensured by BeppoSAX 1–100 keV measurements (Pian et al. 1998) showing a clearly convex spectrum before the synchrotron bump maximum (around 100 keV) which is supposed to be mimicked by the TeV-spectrum before the so-called Inverse-Compton bump maximum. This hypothesis is reinforced by the fact that the sub-TeV slope, which is independent of the CIB density beyond 3.5 μm, effectively reflects the X-ray slope in the keV range. This behaviour (together with the correlated variability reported e.g. by Aharonian et al. 1999a; Djannati-Ataï et al. 1999) indicates that the same population of particles is at the origin of both X-ray and γ-ray emissions, whatever this population is. In particular, the self-synchro-Compton model fits satisfactorily the absorption-corrected data (Guy et al. 2000).

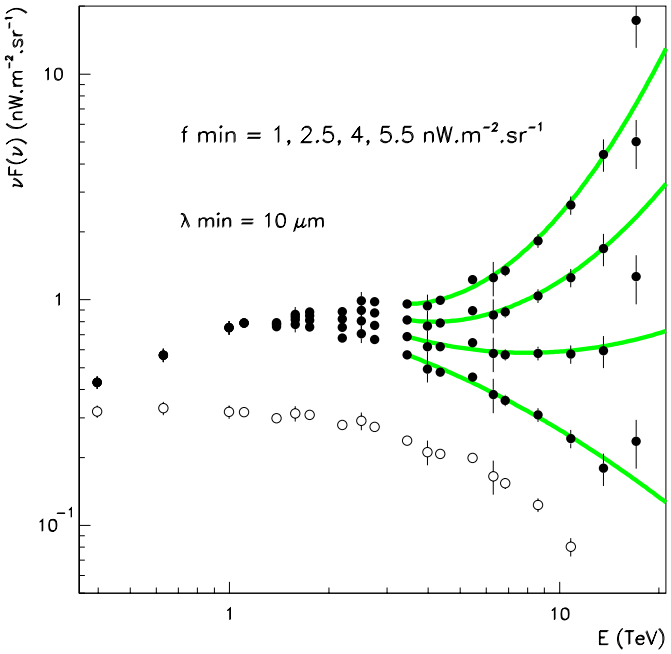

Fig. 2. Shapes of the reconstructed TeV spectra. The open circles show the observed CAT+HEGRA TeV spectrum while the filled symbols show the absorption corrected spectra (*HDF + spectro* hypothesis). The results of the parabola fit are superimposed

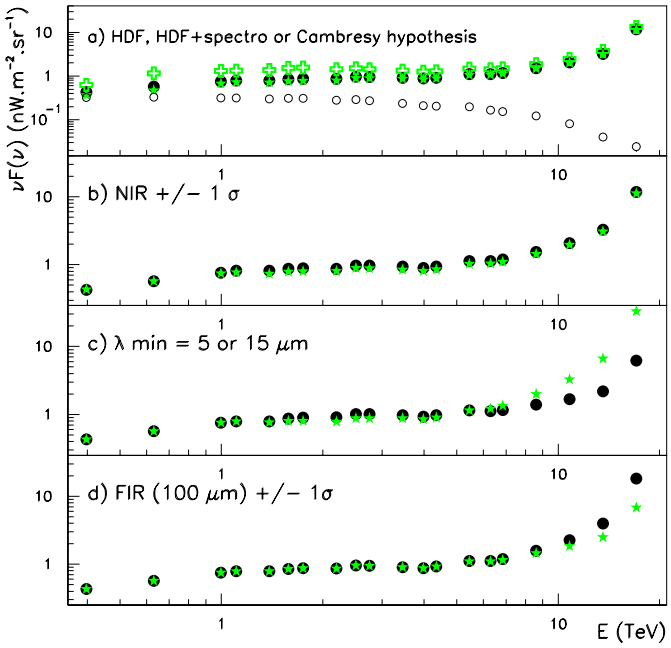

Fig. 3. Impact of the shape of the CIB spectrum on the absorption-corrected TeV spectrum for $f_{\rm min} = 5$ nW m^{-2} sr^{-1}. The open circles (panel **a)**) show the observed TeV spectrum while the other symbols show the absorption-corrected spectra with: **a)** *HDF*, *HDF + spectro* and *Cambresy* hypothesis (resp. stars, filled circles and open crosses); **b)** 3.5 μm value – or + 1 σ (resp. stars and filled circles); **c)** position of the minimum $\lambda_{\rm min} = 5$ or 15 μm (resp. stars and filled circles); **d)** 100 μm value – or + 1 σ (resp. stars and filled circles). By default, $\lambda_{\rm min} = 10$ μm. Error bars are hidden by the experimental points

In order to quantify the concavity of the absorption-corrected spectrum, a parabola fit is performed from 3.3 to 17 TeV in the plane $(\log(\nu), \log(\nu F\nu))$. This function, which is simple, is chosen for its constant second derivative $a = {\rm d}^2(\log(\nu F\nu))/{\rm d}^2(\log(\nu))$, avoids the choice of a particular test-energy and fits satisfactorily the data. The previous physical constraint on the concavity of the TeV spectrum simply reads as $a < 0$. The parameter a is computed for $f_{\rm min}$ in the range 0.1–7 nW m^{-2} s $^{-1}$. Figure 2 shows the result of the parabolic fit in several cases, superimposed on the absorption-corrected experimental points. The fit under-estimates the energy density of the hardest photons, ensuring that the local second derivative is under-estimated and thus making the test conservative.

Furthermore, when $a > 0$, fitted parabola with $-b/2a > 17$ TeV, where $b = {\rm d}(\log(\nu F\nu))/{\rm d}(\log(\nu))$, are accepted. This ensures that, whatever the concavity, no fitted function decreasing with ν over the energy range considered here will be excluded. Asking for a decreasing $\nu F(\nu)$ distribution is the most natural constraint in the previously mentioned (Inverse-Compton bump maximum below or around 1.4 TeV) most favoured case. This double test on both the first and the second derivative makes the resulting upper limit very conservative.

5.2. Reliability of the upper limit

Figure 3 shows the impact of the main uncertainties on the measured part of the CIB density distribution on the absorption corrected TeV spectrum. The observed spectrum of Mkn 501, combining CAT and HEGRA data, is plotted with open circles in panel *a*). Spectra corrected from CIB absorption are superimposed with filled symbols in different cases: *a*) *HDF*, *HDF + spectro* and *Cambresy* hypothesis *b*) 3.5 μm $\pm$ 1 σ (NIR); *c*) position of the minimum $\lambda_{\rm min} = 5$ or 15 μm; *d*) 100 μm value $\pm$ 1 σ (FIR). By default, $\lambda_{\rm min} = 10$ μm.

From panel *a*), it can be seen that the impact of the NIR density below 1 μm is null beyond a few TeV, as the threshold for pair production for a 1 TeV photon is approximately 1 μm. Furthermore, even below 1 TeV, *HDF* and *HDF+spectro* hypothesis lead to the same absorption corrected spectrum. Therefore, only the *HDF + spectro* and *Cambresy* hypothesis will be considered hereafter. The value of $\lambda_{\rm min}$ (panel *c*) and the FIR density at 100 μm – in a minor way – (panel *d*) can slightly change the very high energy tail of the source spectrum (above 10 TeV) while uncertainties on the 3.5 μm measurement have no sizeable impact (panel *b*). So, the uncertainty on the 100 μm measurement and a range of values for the parameter $\lambda_{\rm min}$ (5–15 μm) must be taken into account when deriving upper limits on the MIR density.

The evolution of the parameter a as a function of $f_{\rm min}$ is presented in Fig. 4 in the case $\lambda_{\rm min} = 10$ μm and a *HDF + spectro* CIB density distribution while the values of $f_{\rm min}$ corresponding to a null parameter a (within 5σ)

for several values of $\lambda_{\rm min}$ are gathered in Table 1 for all hypotheses regarding the NIR or the FIR density.

5.3. Conclusion

The results of this work are given in Table 1. The 3.5–100 μm photons being essentially absorbed by 2–15 TeV gamma-rays, the CAT and HEGRA spectra of Mkn 501 are particularly well suited to test the MIR density. The high flux allows a good spectral resolution and the simultaneous X-ray data provides crucial information on the synchrotron bump shape. The MIR upper limit derived in this paper is robust as it is almost independent of the NIR hypothesis (within 1 σ error), and only marginally depends on the FIR flux hypothesis (within 1 σ error). Somewhat more surprising is that the exact position of the minimum in the 5–15 μm range significantly affects the upper limit (as seen in Fig. 3). The quite high sensitivity to the value of $\lambda_{\rm min}$ is due to the fact that the shape of the γ-ray spectrum strongly depends on the CIB density distribution between 5 and 50 μm (and not only on its mean intensity). In other words, more absorption is allowed if the mid-IR spectral distribution, and thus the energy dependence of the extinction, gives an acceptable shape of the TeV spectrum of the source.

This limit is conservative, both due to the method which tends to under-estimate the high energy flux density and to the weak hypothesis regarding the spectrum concavity. Indeed, internal effects, such as Klein-Nishina cut-off and self-absorption, lead to very sharp multi-TeV intrinsic spectra. The upper limit is more constraining than the indirect upper limit derived from the same data on Mkn 501, which relies on a global CIB scaling (Guy et al. 2000). Moreover, whatever the position of the minimum in the range 5–15 μm, the Mid-IR density upper limit remains lower than 4.7 $\mathrm{nW\,m^{-2}\,sr^{-1}}$.

Our results are in agreement with previous works: for example, Stanev & Franceschini (1998) obtained an upper limit of 4 to 5 $\mathrm{nW\,m^{-2}\,sr^{-1}}$ at 15 μm with two CIB hypotheses and Stecker & De Jager (1997) derived an upper limit of 4 $\mathrm{nW\,m^{-2}\,sr^{-1}}$ at 20 μm. It shows the "robustness" of the method based on TeV gamma-rays absorption by IR photons, essentially due to the peak in the pair production cross section. The NIR and FIR fluxes are now confirmed by direct measurements and these observational results enhance the reliability of the constraints on the MIR intensity distribution.

An approach similar to ours has also been proposed by Dwek et al. (2000) who found a CIB density lower than 5 $\mathrm{nW\,m^{-2}\,sr^{-1}}$ in the range 6–30 μm and lower than 10 $\mathrm{nW\,m^{-2}\,sr^{-1}}$ at 60 μm.

6. Discussion on the CIB measurements

6.1. The case of the 60 micron tentative EB detection

From analysis of the DIRBE weekly averaged sky maps, Finkbeiner et al. (2000) have detected substantial flux in the 60 μm DIRBE channel in excess of expected zodiacal and Galactic emission. The observed signal is consistent with an isotropic background at the level $\nu I_\nu = 28.1 \pm 1.8 \pm 7(\mathrm{syst})$ $\mathrm{nW\,m^{-2}\,sr^{-1}}$. While this new excess is not necessarily the CIB, they have ruled out all known sources of emission in the solar system and Galaxy. They therefore tentatively interpret this signal as the CIB. However, they point out that the IR excess exceeds limits on the EB derived from the inferred opacity of the intergalatic medium to observed TeV photons.

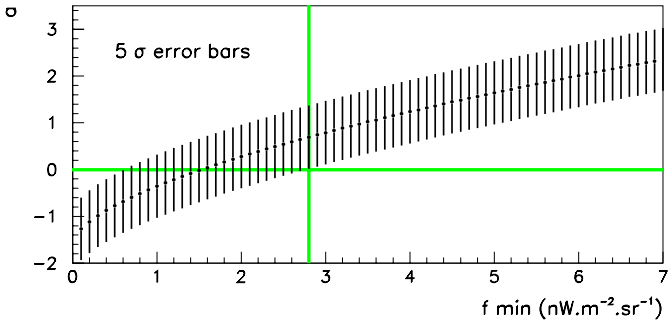

Fig. 4. a parameter of the parabola fit versus $f_{\rm min}$ ($\log(\nu F(\nu)) = a \times \log^2(\nu) + b \times \log(\nu) + c$) with 5 σ errors (for $\lambda_{\rm min} = 10$ μm and a *HDF + spectro* CIB density distribution)

In the assumption that the residual observed at 60 μm is the CIB, we can compute, using the same method as previously, a Mid-IR upper limit on the CIB. With $\lambda_{\rm min} = 10$ μm, we obtain an upper limit of 1.0 $\mathrm{nW\,m^{-2}\,sr^{-1}}$ which is clearly incompatible with the lower limit of 3.3 $\mathrm{nW\,m^{-2}\,sr^{-1}}$ at 15 μm, derived from deep ISOCAM surveys (Biviano et al. 2000). Even when the 60 μm tentative measurement is decreased by 1σ, the absorption-corrected TeV spectrum is unacceptable (upper limit of 1.3 $\mathrm{nW\,m^{-2}\,sr^{-1}}$). With $\lambda_{\rm min} = 15$ μm, the upper limit becomes marginally compatible with the ISOCAM result (upper limit of 2.2 $\mathrm{nW\,m^{-2}\,sr^{-1}}$). Thus, as pointed out by Finkbeiner et al. (2000), we conclude that the 60 μm excess is certainly not only CIB. It contains residual foreground emission, more likely zodiacal residual emission (see Sect. 6.3).

6.2. The EB around 15 μm

Figure 5 shows our results with the 6.5 and 15 μm lower limits obtained by integrating the energy from sources observed in ISOCAM deep fields. The flattening of the faint counts at 15 μm (Metcalfe et al. 2000) suggests that we are now close to convergence and thus that number counts are not very far from the true value of the EB (if no diffuse emission contributes to it). Number counts give 3.3 ± 1.3 $\mathrm{nW\,m^{-2}\,sr^{-1}}$ (Biviano et al. 2000). Using the model of galaxy evolution from Dole et al. (in prep.), we find an EB of about 4.4 $\mathrm{nW\,m^{-2}\,sr^{-1}}$, which is very close to the upper limit derived using the gamma-rays for a high value of $\lambda_{\rm min}$. This tends to show that the absorption in the gamma-ray spectrum of Mkn 501 is mainly, or

Table 1. 5σ upper limit on the Mid-IR density as a function of the position of the minimum $\lambda_{\rm min}$ and of the CIB density distribution

	$5\ \sigma$ Mid-IR density upper limit in $\mathrm{nW\,m^{-2}\,sr^{-1}}$		
IR density	$\lambda_{\rm min} = 5\ \mu$m	10 μm	15 μm
HDF + spectro	1.3	2.8	4.2
Cambresy	1.2	2.6	3.9
100 μm –1 σ	1.8	3.4	4.7
100 μm +1 σ	1.1	2.5	3.9

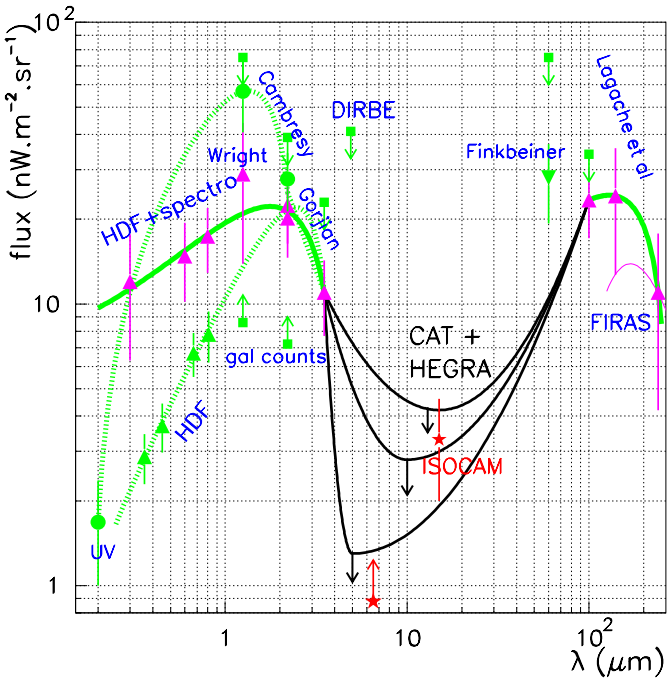

Fig. 5. CIB density as a function of the wavelength: data and upper limits from VHE observation (*HDF + spectro* case). Triangles linked by the wide full grey line indicate the data used in this paper to constrain the NIR and FIR parts: below 3.5 μm the combination of *HDF* measurements and ground-based spectrometry (Bernstein et al. 1999), (Wright 2000) and (Gorjian et al. 2000) points and, above 100 μm, DIRBE results (Lagache et al. 1999). The number counts results from ISOCAM 15 μm (Biviano et al. 2000) and 6.5 μm deep cosmological observations (Désert, private communication) are shown by stars while the squares come from DIRBE/COBE observations (Hauser et al. 1998). The two other hypotheses below 3.5 μm (dotted lines) lead roughly to the same upper limits

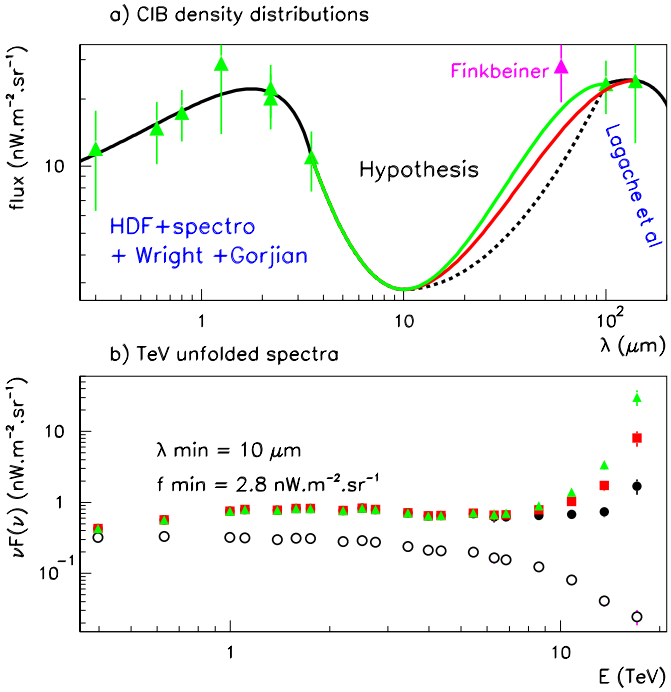

Fig. 6. Consequences of a change in the CIB shape beyond 10 μm: hypothesis on the CIB density distribution (panel **a)**) and corresponding absorption-corrected high energy Mkn 501 spectra (panel **b)**). Ordered by increasing densities, we consider the *normal* (i.e. parabolic) distribution (dots) and two cubic distribution linking the 10 μm minimum to the 140 μm Lagache et al. point (squares) and the 100 μm Lagache et al point (up-triangles)

entirely, due to absorption through electron pair production on CIB photons (see Sect. 7). Thus, the upper limit obtained with $\lambda_{\rm min} = 15\ \mu$m is probably a best guess of the CIB level. Using a different argument based on the expected intrinsic shape of the TeV spectrum and the "high" CIB model from Stecker & De Jager (1998), Konopelko et al. (1999) also concluded that the observed curvature of the spectrum of Mkn 501 could be naturally explained by the extragalactic absorption.

6.3. CIB shape between 10 and 100 μm

In the previous sections, the CIB density distribution was assumed to be described by a parabola between the minimum and the 100 μm Lagache et al. (1999) point. This function may underestimate the EB light and it is important to study the consequences of a change in the CIB shape. As illustrated in Fig. 6, two more realistic (and less conservative) distributions have been tested with a minimum at (10 μm, 2.8 $\mathrm{nW\,m^{-2}\,sr^{-1}}$), i.e. in agreement with ISOCAM measurements. In each case, even taking into account only the 140 μm Lagache et al. point, the shape of the absorption-corrected TeV spectrum is rejected by the physical criteria given in Sect. 5.2. This means that, at least, the 100 μm Lagache et al. (1999) measurement may be overestimated.

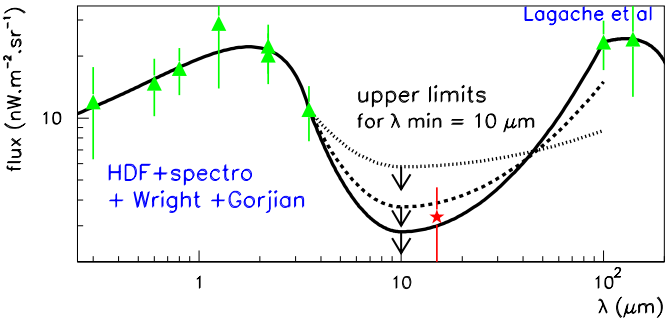

Fig. 7. CIB density vs. wavelength: data and upper limits from VHE observation ($\lambda_{\rm min} = 10$ μm case). The *HDF + spectro* spectrum is linked to different points at 100 μm: Lagache et al. (1999) flux (23.4 $\mathrm{nW\,m^{-2}\,sr^{-1}}$, full line), the same Lagache et al. flux with a higher zodiacal background subtracted (15 $\mathrm{nW\,m^{-2}\,sr^{-1}}$, dashed line) and this point -1σ (8.7 $\mathrm{nW\,m^{-2}\,sr^{-1}}$, dotted line). The number counts result from ISOCAM 15 μm (Biviano et al. 2000) is shown by the star

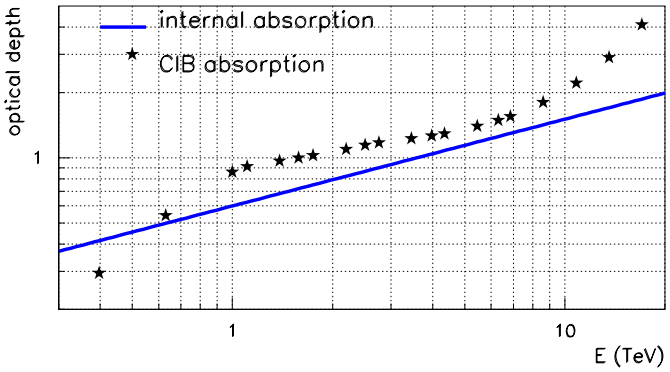

Fig. 8. Optical depth of the TeV flux as a function of the energy E. The stars symbolise the absorption due to the EB photons while the line shows the absorption due to IR photons in the inner jet ($\lambda_{\rm min} = 15$ μm, $f_{\rm min} = 3.3$ $\mathrm{nW\,m^{-2}\,sr^{-1}}$)

The DIRBE zodiacal emission model was obtained by Kelsall et al. (1998) relying on its time variability[2]. This model is critical to obtain the CIB in the near infrared. Its accuracy can be estimated using the residuals observed at wavelengths where the zodiacal emission is maximum (12 and 25 μm). The residual emission, obtained by Hauser et al. (1998), has in fact a spectrum very similar to the zodiacal one. The residuals are about 470 $\mathrm{nW\,m^{-2}\,sr^{-1}}$ at 12 and 25 μm. The work presented just before reveals that this best model may underestimate the zodiacal emission as the uncertainties on other contributions (instrumental and interstellar) are significantly smaller. We can thus make a conservative estimate of the amount of zodiacal emission which is not removed by this model at 12 and 25 μm to be about 400 $\mathrm{nW\,m^{-2}\,sr^{-1}}$. The amount not removed at 60 and 100 μm is thus 40 $\mathrm{nW\,m^{-2}\,sr^{-1}}$ and 8.4 $\mathrm{nW\,m^{-2}\,sr^{-1}}$ (using the Kelsall et al. 1998 smooth high latitude zodiacal cloud colour ratios). This reduces the CIB at 100 μm from 23.4 to 15 $\mathrm{nW\,m^{-2}\,sr^{-1}}$. At 60 μm the extra-zodiacal emission to be removed (40 $\mathrm{nW\,m^{-2}\,sr^{-1}}$) is comparable to the residuals and thus no meaningful value can be obtained on the CIB at this wavelength. Using the same arguments, the extra-zodiacal emission to be removed at 1.25 μm in the Cambrésy et al. (2000) work is 38.0 $\mathrm{nW\,m^{-2}\,sr^{-1}}$ from the published result of 56.9 $\mathrm{nW\,m^{-2}\,sr^{-1}}$.

The impact of a larger zodiacal emission on the upper limits in the MIR range is shown in Fig. 7. With a flatter CIB distribution, the upper limit at 10 μm increases from 2.8 to 3.7 $\mathrm{nW\,m^{-2}\,sr^{-1}}$. It remains very close to the direct measurement from ISOCAM at 15 μm.

In addition to a high interest for cosmology and galaxy evolution, a better knowledge of the entire CIB shape would be of great interest to unfold TeV spectra of extragalactic sources.

[2] Other more empirical models have also been built by Wright (2000) and Finkbeiner et al. (2000).

7. Discussion on Mkn 501 physical parameters

In the previous section, so as to derive a conservative upper limit on the CIB density, no internal absorption within the source has been taken into account. Nevertheless, the ISOCAM 15 μm point (at 3.3 $\mathrm{nW\,m^{-2}\,sr^{-1}}$) gives a lower limit on the CIB density and, assuming this value to be a measurement, the resulting maximum possible absorption within the source can be estimated. The previous physical constraints on the absorption corrected spectrum can be applied again, assuming the minimum possible CIB density (to remain conservative), and varying the optical depth $\tau_{\rm AGN}$ due to $\gamma - \gamma$ pair production within the jet of Mkn 501.

To compute $\tau_{\rm AGN}$ in the TeV range, the low-energy spectrum (i.e. the energy distribution of target photons) has to be known. We use the approximation derived by (Bednarek & Protheroe 1999) using a fit of the BeppoSAX observations made during the April 15/16 flaring activity together with an indication from OSSE observation made during the high state in 1997 April that the spectrum continued to approximately 500 keV with the same energy flux per log energy interval. Performing a numerical integration of the optical depth formula (cf. Sect. 4), the authors show that, in the framework of homogeneous SSC model:

$$\tau_{\rm AGN} \approx 3\ 10^{8} D^{-4.8} E^{0.4} t_{\rm var}^{-1}$$

where D is the Doppler factor of the blob where relativistic electrons are assumed to be confined, $t_{\rm var}$ is the variability time-scale of the source in seconds and E is the γ-rays energy in TeV. The efficiency usually associated with this mechanism has been supposed, as usual, equal to unity.

Both absorptions are compared in Fig. 8. They look rather similar as the dominant behaviour is in E^{-2} in energy density. However, the internal absorption is continuously increasing with energy while the CIB absorption exhibits a "plateau" around 1–4 TeV. Adding this new optical depth to the one associated with $\gamma-$CIB interactions, we derive a 5σ upper limit for $3\ 10^{8} D^{-4.8} t_{\rm var}^{-1}$ of 0.6 (computed with $\lambda_{\rm min} = 15$ μm and $f_{\rm min} = 3.3$ $\mathrm{nW\,m^{-2}\,sr^{-1}}$,

i.e. for the ISOCAM point). With a reasonable variability time-scale around 1 hour, the resulting minimum Doppler factor is $D > 11.7$. Despite the large CIB absorption and the resulting stringent upper limit on the internal optical depth, these Doppler factors are in agreement with classical AGN descriptions and the simple homogeneous SSC model works satisfactorily. Nevertheless, it should be pointed out that this lower limit on the Doppler factor increases as the wavelength of the minimum of CIB density decreases and becomes infinite below $\approx 10\ \mu m$ when there is no space left for internal absorption, unless an inhomogeneous jet is assumed.

With the next generation of instruments (VERITAS and MAGIC in the northern hemisphere, HESS and CANGAROO in the southern one) which will start operating in 2002/2003, good quality spectra of several AGNs at different redshifts, will be available. It will lead to, simultaneously, a better understanding of the TeV emission mechanism and a better knowledge of the CIB density distribution.

Note added in proof: In this paper an early version of the Cambrésy et al. (2000) paper was used: the 1.25 μm flux was overestimated by 5%; it does not affect our results.

Acknowledgements. The authors appreciate the contribution of the anonymous referee to the improvement of the paper. We are grateful to H. Krawczynski who provided us with numerical values of HEGRA fluxes and with W. Bednarek for very helpful discussions.

References

Aharonian, F. A., Akhperjanian, A. G., Barrio, J. A., et al. 1997, A&A, 327, L5
Aharonian, F. A., Akhperjanian, A. G., Barrio, J. A., et al. 1999a, A&A, 342, 69
Aharonian, F. A., Akhperjanian, A. G., Barrio, J. A., et al. 1999b, A&A, 349, 11
Aharonian, F. A. 2000, New Astron., 5, 277
Armand, C., Milliard, B., & Deharveng, J. M. 1994, A&A, 284, 12
Barrau, A. 1998, Ph.D. Thesis, Université J. Fourier, Grenoble, France
Bednarek, W., & Protheroe, R. J. 1999, A&A, 310, 577
Bernstein, R. A., Freedman, W. L., & Madore, B. F. 1999, preprint
Biller, S. D., Buckley, J., Burdett, A., et al. 1998, Phys. Rev. Let., 80, 2992
Biviano, A., Metcalfe L., Altieri, B., et al. 2000, Lustering at High Redshift, ASP Conf. Ser., 200, ed. A. Mazure, O. Le Fèvre, & V. Le Brun
Bowyer, S. 1991, ARA&A, 29, 59
Cambrésy, L., Reach, W. T., Beichman, C. A., & Jarrett, T. H. 2000, accepted for publication in ApJ
Catanese, M., Bradbury, S. M., Breslin, A. C., et al. 1997, ApJ, 487, L143
Coppi, S., & Aharonian, F. A. 1999, ApJ, 521, L33
Djannati-Ataï, A., Piron, F., Barrau, A., et al. 1999, A&A, 350, 17
Dwek, E., & Arendt, R. G. 1998, ApJL, 508, L9
Dwek, E., et al. 2000, IAU, 204, 46
Elbaz, D., Aussel, H., Césarsky, C. J., et al. 1998, in The Universe as seen by ISO, ed. P. Cox, & M. F. Kessler, UNESCO, Paris, ESA Special Publications series (SP-427)
Finkbeiner, D. P., Davis, M., & Schlegel, D. J. 2000, ApJ, 544, 81
Fixsen, D. J., Dwek, E., Mather, J. C., Bennett, C. L., & Shafer, R. A. 1998, ApJ, 508, 123
Funk, B., et al. 1998, APh, 9, 97F
Gispert, R., et al. 2000, A&A, 360, 1
Gorjian, V., Wright, E. L., & Chary, R. R. 2000, ApJ, 536, 550
Gould, J., & Schreder, G. 1967, Phys. Rev., 155.5, 1404
Guy, J., Renault, C., Aharonian, F., Rivoal, M., & Tavernet, J.-P. 2000, A&A, 359, 419
Hayashida, N., Hirasawa, H., Ishikawa, F., et al. 1998, ApJ, 504, 71
Hauser, M. G., Arendt, R. G., Kelsall, T., et al. 1998, ApJ, 508, 25
Heitler, W. 1960, The Quantum Theory of Radiation, Oxford
Kelsall, T., Weiland, J. L., & Franz, B. A. 1998, ApJ, 508, 44
Konopelko, A. K., Kirk, J. G., Stecker, F. W., & Mastichiadis, A. 1999, ApJ, 518, L13
Lagache, G., Haffner, L. M., Reynolds, R. J., & Tufte, S. L. 1999, A&A, 354, L247
Lamer, G., & Wagner, S. J. 1998, A&A, 331, L13
Macminn, D., & Primack, J. R. 1996, Space Sci. Rev., 75, 413M
Malkan, M. A., & Stecker, F. W. 1998, ApJ, 496, 13M
Metcalfe, L., et al. 2000, The Extragalactic Infrared Background and its Cosmological Implications, IAU Symp., No. 204
Nikishov, A. I. 1962, Sov. Phys. JEPT, 14, 2
Pian, E., Vacanti, G., Tagliaferri, G., et al. 1998, ApJ, 492, L17
Pozzetti, L., Madau, P., Zamorani, G., Ferguson, H. C., & Bruzual, A. G. 1998, MNRAS, 298, 1133
Samuelson, F. W., Biller, S. D., Bond, I. H., et al. 1998, ApJ 501, L17
Samuelson, F. W., Biller, S. D., Bond, I. H., & Boyle, P. J. 1998, ApJ, 501, L17
Schlegel, D. J., Finkbeiner, D. P., & Davis, M. 1998, ApJ, 500, 525
Stanev, T., & Franceschini, A. 1998, ApJ, 494, L159
Stecker, F. W. 1999, APh, 11 (1-2), 83
Stecker, F. W., & De Jager, O. C. 1998, A&A, 334, L85
Stecker, F. W., & De Jager, O. C. 1997, Proc. Kruger Park TeV Gamma-ray Conf. [astro-ph/9710145]
Stecker, F. W., De Jager, O. C., & Salamon 1992, ApJ, 390, L49
Wright, E. L. 2000 [astro-ph/0004192]